International Journal of Pharmaceutics 426 (2012) 248–255

Contents lists available at SciVerse ScienceDirect

International Journal of Pharmaceutics

journal homepage: www.elsevier.com/locate/ijpharm

Pharmaceutical Nanotechnology

Novel superparamagnetic iron oxide nanoparticles for tumor embolization application: Preparation, characterization and double targeting

Xiaoli Chen[1], Haiyan Lv[1], Min Ye, Shengyu Wang, Erru Ni, Fanwei Zeng, Chang Cao, Fanghong Luo*, Jianghua Yan**

Cancer Research Center, Medical College, Xiamen University, 422 Siming South Road, Xiamen, Fujian 361005, China

ARTICLE INFO

Article history:
Received 4 November 2011
Received in revised form 14 January 2012
Accepted 19 January 2012
Available online 30 January 2012

Keywords:
Magnetic nanoparticles
Superparamagnetic
o-Carboxymethylchitosan
Truncated tissue factor
Tumor targeting

ABSTRACT

The goal of this study was to develop novel embolic nanoparticles for targeted tumor therapy with dual targeting: magnetic field-guided and peptide-directed targeting. The embolic nanoparticles SP5.2/tTF-OCMCs-SPIO-NPs were prepared by surface-modifying of superparamagnetic iron oxide nanoparticles (SPIO-NPs) with *o*-carboxymethylchitosans (OCMCs) and SP5.2/tTF (SP5.2: a peptide binding to VEGFR-1; tTF: truncated tissue factor) to improve their stability and to target over-expressing VEGFR-1 cells. The physicochemical characterization results showed that the OCMCs-SPIO-NPs have a spherical or ellipsoidal morphology with an average diameter of 10–20 nm. And they possess magnetism with a saturation magnetization of 66.1 emu/g, negligible coercivity and remanence at room temperature. In addition, the confocal microscopy, Prussian blue staining and FX activation analysis respectively demonstrated the peptide-directed targeting, magnetic field-guided targeted and blood coagulation activity of the SP5.2/tTF-OCMCs-SPIO-NPs. These properties separately belong to SP5.2, Fe_3O_4 and tTF moieties of the SP5.2/tTF-OCMCs-SPIO-NPs. Thus these SP5.2/tTF-OCMCs-SPIO-NPs with double-targeting function should have a potential application in embolization therapy of tumor blood vessels.

1. Introduction

The neo-angiogenesis is an absolute requirement for the progression of malignant neoplasms because it provides sufficient supply of oxygen and nutrients as well as elimination of waste products (Carmeliet, 2000; Folkman, 1995; Folkman et al., 1989; Hanahan and Folkman, 1996). Selective inducing local thrombosis in tumor blood vessels with subsequent tumor infarction is a promising anticancer strategy (Huang et al., 1997). A potential mediator of this event is tissue factor (TF), which is the initiator of the extrinsic pathway of the blood coagulation cascade (Furie and Furie, 1988). The extracellular domain of TF (truncated tissue factor, tTF) is not a coagulant while free in the blood circulation but becomes a powerful and specific coagulant once bound to the cell surface of the tumor vasculature by a targeting peptide (Morrissey et al., 1993; Stone et al., 1995). Thereby, a variety of fusion proteins consisting of the tTF fused to the peptides GRGDSP (abbr. RGD), GNGRAHA (abbr. NGR), NGYEIEWYSWVTHGMY (abbr. SP5.2) or derivatives of these peptides have been synthesized (Goncalves et al., 2007a; Schwoeppe et al., 2010). The peptide SP5.2 could be used to mediate specific binding to VEGFR-1 (Flt-1), which generally over-express on the neo-vascular endothelial cell surface (Goncalves et al., 2007b). However, these fusion proteins like SP5.2/tTF usually could not induce the complete thrombosis because these events determine not only by the specificity of the delivery moiety but also by the population and distribution of their target (antigens or receptors), which restrict the concentration of tTF at the tumor blood vessels (Hu et al., 2003b). In order to enhance the local accumulation and retention of the effector tTF at tumor blood vessels, in this study, we introduce a potential effective mediator magnetic nanoparticle.

Superparamagnetic iron oxide nanoparticles (SPIO-NPs) encompass various desirable features that have been broad applied in magnetic resonance imaging (MRI), targeted drug delivery and hyperthermia (Corot et al., 2006; Ito et al., 2005; Schweiger et al., 2011). Especially, the superparamagnetism of SPIO-NPs allow them to be guided with an external magnetic field, which is critical for using in pharmaceutical and biomedical applications (Lei et al., 2009). Thus the SPIO-NPs could be accumulated and fixed at the desired target area *via* an external magnetic field (Jain et al., 2005). However, the bare iron oxide magnetic nanoparticles are likely to form a large aggregation, alter magnetic properties, and will undergo rapid biodegradation when they are directly exposed to the biological system (Shubayev et al., 2009). Therefore, it is

* Corresponding author. Tel.: +86 592 2187750; fax: +86 592 2186731.
** Corresponding author. Tel.: +86 592 2180587; fax: +86 592 2186731.
E-mail addresses: luofanghong@xmu.edu.cn (F. Luo), jhyan@xmu.edu.cn (J. Yan).
[1] These authors contributed equally to this work.

0378-5173/$ – see front matter © 2012 Elsevier B.V. All rights reserved.
doi:10.1016/j.ijpharm.2012.01.043

essential to surface-modify the bare nanoparticles with hydrophilic polymers such as dextran, chitosan, *o*-carboxymethylchitosan (OCMC) (Lind et al., 2002; Zhu et al., 2008). OCMC which is a water-soluble chitosan derivative, has abundant amino groups and carboxyl groups which can effectively attach to different substances like antibodies or peptides. In addition, the OCMCs could not only stabilize nanoparticles *via* covalent or non-covalent surface modification but also could control the mean size of the nanoparticles in 10–100 nm to escape rapid renal clearance and capture by the reticuloendothelial system (Berry et al., 2004).

And therefore, in this study, we describe a simple method to synthesize the novel embolic nanoparticles SP5.2/tTF-OCMCs-SPIO-NPs in two steps. The SPIO-NPs with stability and abundant functional groups were prepared by OCMCs surface modification (thereafter called OCMCs-SPIO-NPs). Then, the fusion proteins SP5.2/tTF with the blood coagulation activity were cross-linked to OCMCs-SPIO-NPs by electrostatic adsorption or covalent binding. The final product SP5.2/tTF-OCMCs-SPIO-NPs were investigated the effects of the peptide-directed targeting, magnetic field-guided targeted and blood coagulation.

2. Materials and methods

2.1. Materials

Nickel-nitrilotriacetic acid (Ni-NTA) agarose were purchased from Qiagen (USA). Ferric chloride ($FeCl_3{\cdot}6H_2O$), ferrous sulfate ($FeSO_4{\cdot}7H_2O$), aqueous ammonia (25 wt.%), were purchased from Shanghai Reagent Company of China. *o*-Carboxymethyl chitosan (MW 1–2 million, deacetylation degree ≥ 93%, carboxyl group to replace the degree of ≥87%) was purchased from Zhejiang Sendai Chitosan Co., Ltd., Dulbecco's modified Eagle's medium (DMEM), GIBCO fetal bovine serum were purchased from Invitrogen-Life Technologies. All chemicals are analytical graded and used without further purification. The ultra-pure water was used during the whole study.

2.2. Expression and purification of the fusion proteins SP5.2/tTF

The expression vector encoding the fusion proteins SP5.2/tTF has been successfully constructed in our laboratory. These plasmids were introduced in competent *E. coli* cells (BL21, DE3) according to the manufacturer's protocol. The bacteria were cultivated in Luria broth medium supplemented with ampicillin (0.1 mg/ml). When the bacteria cell suspensions reached an OD of −0.5, over-expression of the fusion proteins was initiated by adding isopropyl-L-thio-B-D-galactopyranoside (IPTG). After stimulating with IPTG, the cells were harvested and 5 ml lysis buffer (20 mmol/l Tris–HCl, pH 8.0; 0.5 mol/l NaCl; 1 mmol/l EDTA; 1 mg/ml lysozyme) per gram wet weight were added. Then the cells were incubated for 90 min and centrifuged at 12,000 × *g* for 15 min at 4 °C. The pellet was resuspended and homogenized by sonicating in washing buffer (20 mmol/l Tris/HCl, pH 8.0; 0.5 mol/l NaCl; 2 mol/l urea; 20 ml/l Triton X-100). To solubilize the inclusion bodies, 5 ml solution buffer (20 mmol/l Tris/HCl, pH 8.0; 8 mol/l urea; 1 mmol/l β-mercaptoethanol; 20 ml/l Triton X-100) per gram wet weight were added. After incubation overnight at room temperature, the suspension was centrifuged at 12,000 × *g* for 30 min at 4 °C. The supernatant was loaded onto a nickel-nitrilotriacetic acid (Ni-NTA) column for purification. The purification and refolding were done with the His Bind Buffer kit according to the manufacturer's protocol and subsequent dialysis of the IMAC eluate (to phosphate buffer solution, PBS) in a dialysis cassette. The final products were analyzed under denaturing conditions on SDS-PAGE.

2.3. Preparation of OCMCs-SPIO-NPs

The OCMCs-SPIO-NPs were prepared by alkaline co-precipitation of ferric chlorides ($FeC1_3{\cdot}6H_2O$), ferrous sulfate ($FeSO_4{\cdot}7H_2O$) and OCMCs solution in anaerobic conditions (Hong et al., 2008a; Molday and MacKenzie, 1982). A brief description of the procedure was as follows. The mixture of OCMCs and $FeC1_3{\cdot}6H_2O$ was dissolved into deionized water and stirred under a flow of nitrogen. Then, $FeSO_4{\cdot}7H_2O$ with molar ratio of 2:1 to $FeC1_3{\cdot}6H_2O$ was added and dissolved completely. The ammonia solution was quickly dropped into above mixture with vigorous stirring, at a controlled pH (10–11). The resulting solution was incubated for 60 min and cooled down. Then the products were purged by centrifuge (2000 rpm) for 10 min to separate large particles from the solution. The liquid at the top of the separation tube was dialysis to ultrapure water for 24 h using a dialysis cassette. Excess ammonia, iron cation and OCMC macromolecules should be removed. And, the OCMCs-SPIO-NPs powder were obtained by drying in vacuum at 60 °C for subsequent functionalization with proteins.

2.4. Characterization

2.4.1. X-ray diffraction (XRD)

To confirm the presence of crystalline Fe_3O_4 nanoparticles, the crystal structures of SPIO-NPs and OCMCs-SPIO-NPs were examined on a powder XRD. Pattern of the each sample was recorded with the Panalytical X'pert PRO X-ray diffractometer using Cu Kα radiation (λ = 1.5406 Å). A continuous scan mode was used to collect 2θ data from 10° to 90°. The distances between peaks were compared to the JCPDS 88-0315 of International Center for Diffraction Data to determine crystal structures.

2.4.2. Scanning electron microscopy (SEM)

The particle size and morphology of SPIO-NPs and OCMCs-SPIO-NPs were inspected on a HITACHI S-4800 field emission scanning electron microscope. The nanoparticle powders were diluted in PBS with the aid of ultrasonic (500 W). The SEM samples were prepared by dropping dilute suspension on the glass and the surface was coated with a thin gold film under vacuum prior to the microscopy.

2.4.3. Fourier transform infrared (FTIR) spectroscopy

The compositions of the samples were examined by Fourier transform infrared (FTIR) spectroscope. Measurements of uncoated SPIO-NPs powder, pure OCMCs and OCMCs-SPIO-NPs powder were performed with pressed pellets that were made by using KBr powder as diluent. Each sample (5 mg) was thoroughly mixed and crushed with the 500 mg of KBr using a mortar and pestle. The mixture (80 mg) was placed in a pellet former and was pressurized for 2 min to form the KBr pellet. The FTIR spectrum was collected between the wave number of 400 and 4000 cm^{-1} using a Nicolet Avatar 360 Fourier transform infrared spectrometer with a resolution of 4 cm^{-1}.

2.4.4. Magnetization measurements

The dried samples were further investigated with regard to their expected superparamagnetic behavior. Small amounts of material were introduced into a Magnetic Property Measurement System MPMS® equipped with 5 T magnet (Quantum Design, San Diego, CA) using superconducting quantum interference device (SQUID) technology. The samples underwent an external magnetic field from +3000 Oe to −3000 Oe at 300 K in order to generate hysteresis loops.

2.5. SP5.2/tTF conjugated to OCMCs-SPIO-NPs

The OCMCs-SPIO-NPs powder was dispersed in 5% glutaraldehyde containing PBS (pH 6.8) at a Fe concentration of 5 mg/ml and kept at room temperature for 10 h. The nanoparticles were separated by a strong magnetic field and then washed three times with water. Next, the fusion proteins SP5.2/tTF diluent solution in PBS (pH 7.4) was added to the particles and the conjugation reaction was carried out at 4 °C for 4 h in a shaker at 200 rpm. After that, the SP5.2/tTF-conjugated OCMCs-SPIO-NPs were recovered by a magnetic separation, washed with PBS at pH 7.4 to remove unbound proteins. The supernatant solution was used to detect the amount of unbound proteins by the Bradford method. The SP5.2/tTF-OCMCs-SPIO-NPs were stored at 4 °C for later use.

2.6. Functional studies of SP5.2/tTF-OCMCs-SPIO-NPs

2.6.1. Cell culture

HUVECs (human umbilical vein endothelial cells) and SMMC-7721 cells (a human liver cancer cell line that over-express VEGFR-1) were chosen for *in vitro* experiments (Ai et al., 2008; Gille et al., 2001). The SMMC-7721 cells were cultured in high glucose Dulbecco's modified Eagle's medium (DMEM) supplemented with 10% fetal bovine serum (FBS) and 1% penicillin–streptomycin. Human umbilical vein endothelial cells (HUVECs) were cultured in low glucose DEME supplemented with human epidermal growth factor and 10% FBS. And all the cells were routinely cultured at 37 °C in a humidified atmosphere with 5% CO_2 (in air).

2.6.2. Confocal microscopy

HUVECs (2×10^5 cells in 2 ml medium) were seeded into a 12-well culture plate containing one glass coverslip/well and incubated. When cells reached 60% cloning efficiency, the supernatant was removed and cells were washed three times with PBS (pH 7.4). Afterwards, 2 ml of the full culture medium containing the fusion proteins SP5.2/tTF, SP5.2/tTF-OCMCs-SPIO-NPs and OCMCs-SPIO-NPs (iron concentration of 0.4 mg/ml) was added, respectively. Referred SP5.2/tTF has been pre-labeled with Rhodamine B isothiocyanate (RBITC). After incubated in the dark for 1, 6 and 12 h respectively, the coverslips with cells were placed in empty wells, treated with 1 ml of 4% paraformaldehyde in PBS for 30 min, and washed three times with PBS. The slides were mounted with the nuclear stain, Hoechst 33258, then examined under the fluorescence microscope and photographed.

2.6.3. Prussian blue staining

The influence of magnetic field on cell uptake of MNPs was visualized using Prussian blue staining. SMMC-7721 cells (5×10^5 cells in 4 ml medium) were seeded in 60 mm Petri dish. After incubation for 24 h, a predetermined amount of SP5.2/tTF-OCMCs-SPIO-NPs in medium was added into dish to adjust for a Fe concentration of 0.5 mg/ml. A masterly experiment was designed as a cylindrical 0.6 T magnet was placed against the outer bottom wall of the Petri dish at different distances (*i.e.* 0 cm, 1 cm and 2 cm, respectively) to vary the magnetic field strength applied to the cells (Yang et al., 2008). After incubation for 6 h, the cells were washed twice with PBS, fixed by adding 4 ml of 4% paraformaldehyde containing PBS for 30 min. At last the cells were stained with Prussian blue. Each dish received a 2.5 ml of a 2:1 (v/v) mixture of 2% potassium ferrocyanide(II) trihydrate and 2% HCl solutions, after which cells were incubated for 20 min at 37 °C. Cells were then washed three times with PBS, and the Prussian blue staining results were assessed on an inverted fluorescence microscope and photographed.

2.6.4. Factor X coagulation assay

To verify the blood coagulation abilities of the tTF moiety of SP5.2/tTF or SP5.2/tTF-OCMCs-SPIO-NPs, a Factor X activation assay was performed as described by Ruf et al. (1991). Briefly, various concentrations (0.01–100 μmol/l) of SP5.2/tTF or SP5.2/tTF-OCMCs-SPIO-NPs were mixed with 100 nmol/l Factor VII in Tris-buffered saline buffer and incubated at 37 °C for 10 min, to which 5 nmol/l Factor X was added. The mixture was then incubated at room temperature for another 10 min, to which 100 mmol/l EDTA were added to quench the reaction. Thereafter, 2 nmol/l chromogenic substrate Spectozyme Factor Xa was added, and the mixture read at 405 nm in the first 5-min time period.

2.6.5. Histology analysis

BALB/c nude male mice, 4–6 weeks old, were obtained from the Experimental Animal Center of Xiamen University in China. One million SMMC-7721 cells were suspended in 200 μl of serum free medium and injected subcutaneously into one side of mice. When tumor reached an average size of 1.0 cm^3, the mice were randomly assigned to the different treatment groups: (1) PBS (the control group), (2) the fusion proteins SP5.2/tTF, (3) SP5.2/tTF-OCMCs-SPIO-NPs (0.2 ml, 5 mgFe/ml) with an external magnetic field. Nd–Fe–B magnets, 0.6 T, were fixed externally touching the mice skin without causing pressure (Krukemeyer et al., 2011).

To assess the extent and location of thrombosis in SP5.2/tTF-OCMCs-SPIO-NPs treated mice, tumors were collected at 48 h after injection, embedded in embedding medium for cryosections, sectioned, and stained with H&E. Thrombosis of vessels was assessed as either total or incomplete depending on the extent of closely packed erythrocytes, blurring of the vessel outline, and the presence of aggregated platelets and fibrin deposition (Hu et al., 2003a).

3. Results and discussion

3.1. Expression and purification of fusion proteins SP5.2/tTF

SDS-PAGE analysis in Fig. 1a shows the expressions of SP5.2/tTF induced using various concentrations (0–1 mmol/l) IPTG. When 0.6 mmol/l IPTG were added, the proteins yield reached maximum. Fig. 1b demonstrated that the fusion proteins were mostly expressed in the form of inclusion bodies. These inclusion bodies could be solubilized in denaturing buffer and purified by nickel affinity chromatography, and the purified proteins were further detected and identified by SDS-PAGE. As Fig. 1b shows there are nearly no impure proteins after the purification and the objective protein is about 35 kDa which nearly approach to the theoretical reference value.

3.2. Physicochemical characterization of OCMCs-SPIO-NPs

3.2.1. X-ray diffraction (XRD)

Fig. 2 shows the XRD patterns for SPIO-NPs (Fig. 2a) and OCMCs-SPIO-NPs (Fig. 2b). The positions and relative intensities of the diffractograms agree well with those XRD patterns of Fe_3O_4 nanoparticles in literatures, which confirm the structure of the magnetite materials (JCPDS card no. 88-0315) (Hong et al., 2008b; Liu et al., 2005). The characteristic peaks at $2\theta = 30.1°$, 35.5°, 43.1°, 53.4°, 57.0°, 378° and 62.6° for naked SPIO-NPs (Fig. 2a), which were marked, respectively, by their indices (2 2 0), (3 1 1), (4 0 0), (4 2 2), (5 1 1), and (4 4 0), were also observed for OCMCs-SPIO-NPs (Fig. 2b). This result indicates that Fe_3O_4 magnetite nanoparticles were still incorporated in the composite particles OCMCs-SPIO-NPs and there is little influence in the phase change of the amorphous OCMCs as a dispersant on the structure of SPIO-NPs.

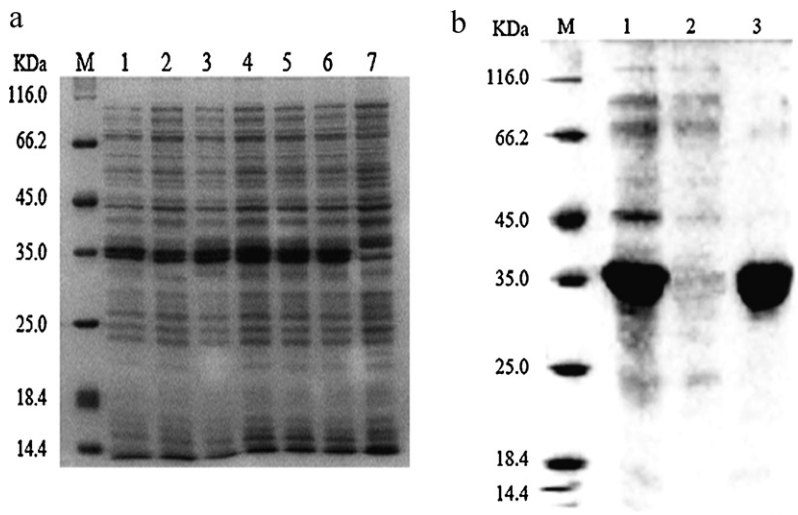

Fig. 1. (a) SDS-PAGE analysis for the expression of the fusion protein SP5.2/tTF in *E. coli* cells (BL21, DE3). M, protein marker; lanes 1–6, total protein from BL21(DE3) with 0.1 mmol/l, 0.2 mmol/l, 0.4 mmol/l, 0.6 mmol/l, 0.8 mmol/l and 1 mmol/l IPTG induction, respectively; lane 7, total protein from BL21(DE3) without induction. (b) SDS-PAGE analysis for the purity of SP5.2/tTF. M, protein marker; lane 1, the precipitate of the bacteria cell suspensions after lysis and ultrasonic treatment; lane 2, the supernatant of the bacteria cell suspensions after lysis and ultrasonic treatment; lane 3, SP5.2/tTF purified by Ni-NTA column.

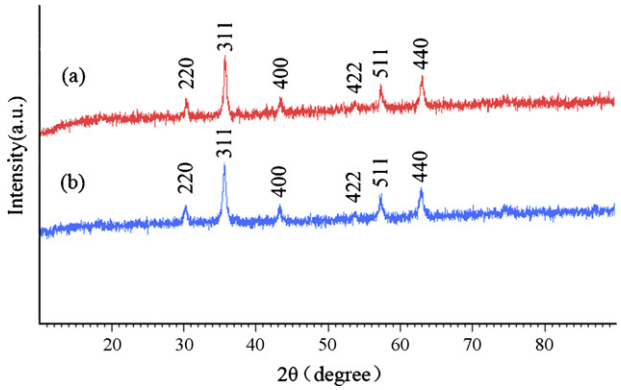

Fig. 2. X-ray diffraction (XRD) patterns of uncoated SPIO-NPs (a) and OCMCs-SPIO-NPs (b).

3.2.2. Scanning electron microscopy (SEM)

Fig. 3a is a SEM image of the synthesized OCMCs-SPIO-NPs, which shows that most of the particles are quasi-spherical or ellipsoidal with an average diameter of 10–20 nm. By comparison, Fig. 3b shows the SEM image of uncoated SPIO-NPs, which shows a more serious aggregate phenomenon than the OCMCs-SPIO-NPs in Fig. 3a. This is because the specific surface area (surface-to-volume ratio) is large and the surface energy is high, SPIO-NPs are apt to aggregate during the process of filtration and drying. However, after OCMCs coating, improvement of the aggregate phenomenon was observed. In addition, little change of the nanoparticles in the size was seen when nanoparticles underwent surface functionalization by OCMCs. It implied that the coupling of polymer would not significantly work on the thickness of the coating.

3.2.3. Fourier transform infrared (FTIR) spectroscopy

Fig. 4 shows the FTIR spectra for uncoated SPIO-NPs (Fig. 4a), OCMCs (Fig. 4b) and OCMCs-SPIO-NPs (Fig. 4c). The analysis indicated absorption centered at 573 cm^{-1} corresponding to the Fe–O vibration related to the magnetite phase. The presence of additional peaks centered at 1417 cm^{-1} and 1589 cm^{-1} was most probably due to the symmetric and asymmetric stretching vibration of carboxyl groups, respectively. Compared with SPIO-NPs (Fig. 4a) and OCMCs-SPIO-NPs (Fig. 4c), the peak at 573 cm^{-1} was blue-shifted to 585 cm^{-1}, which demonstrated that the formation of new bonds between the SPIO-NPs and OCMCs. And the bending band at 1654 cm^{-1} and 3440 cm^{-1} could be ascribed to the —OH groups, Fig. 4a showed the surface of SPIO-NPs have large numbers of hydroxyl which should be utilized to covalently bind OCMCs (Zhou et al., 2006). The peak of 1410 cm^{-1} and 1609 cm^{-1} at the OCMCs-SPIO-NPs (Fig. 4c) indicated a complex reaction between carboxyl

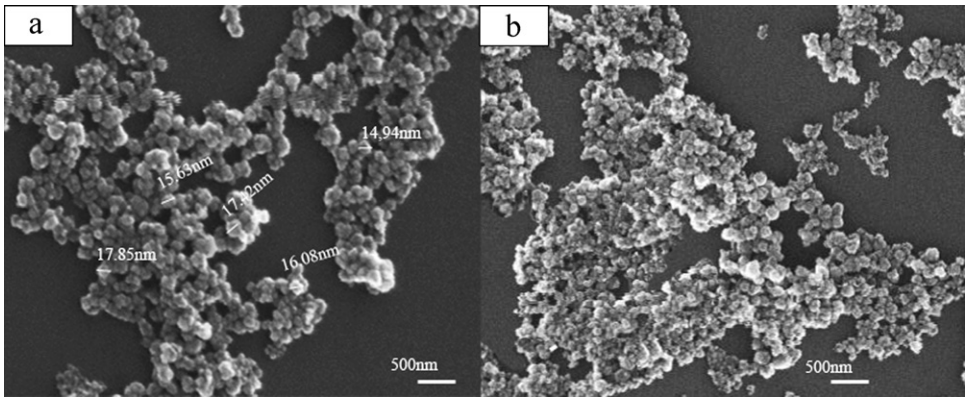

Fig. 3. SEM images of the uncoated SPIO-NPs (a) and OCMCs-SPIO-NPs (b).

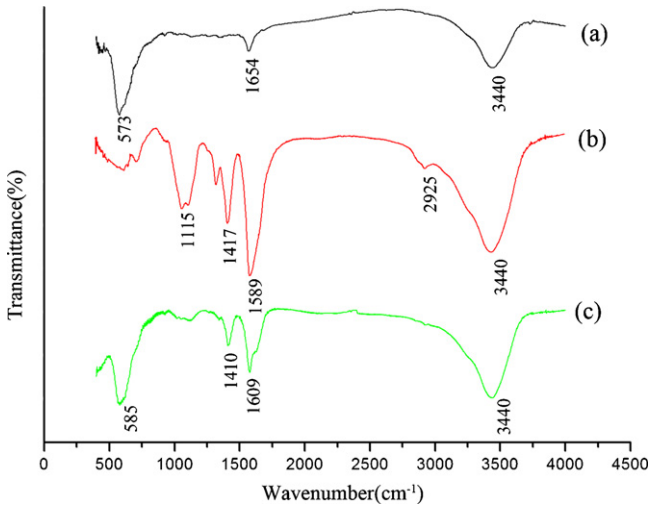

Fig. 4. Fourier transform infrared (FTIR) spectra of synthesized SPIO-NPs (a), OCMCs (b) and OCMCs-SPIO-NPs (c).

groups of OCMCs and hydroxy groups on the surface of SPIO-NPs. The peak of —C—O—C— at 1391 cm^{-1} was observed at OCMCs-SPIO-NPs (Fig. 4c), which can also be assigned to the cross-linked OCMCs. Overall, these FTIR spectra provided supportive evidence that OCMCs were successfully modified onto the SPIO-NPs surface.

3.2.4. Magnetic properties

Fig. 5 shows the magnetization hysteresis loops of uncoated SPIO-NPs (Fig. 5a) and OCMCs-SPIO-NPs (Fig. 5b). The saturation magnetic moments of OCMCs-SPIO-NPs reached 61.1 emu/g. This saturation magnetization values was slightly less than the reference value for the uncoated SPIO-NPs (66.1 emu/g). This can be explained by considering the presence of OCMC polymer shells. In addition, there is no remanence at low magnetic field from the hysteresis loops, so the coercivity is almost negligible in the absence of an external magnetic field. It indicated that SPIO-NPs and OCMCs-SPIO-NPs both possess superparamagnetic properties at room temperature. When the size of prepared Fe_3O_4 nanoparticles is less than the critical size of superparamagnetism, they will bring forth superparamagnetism, because they are so small that each particle is a single magnetic domain and its spin reversal energy barrier is easily overcome by thermal vibrations. These magnetic

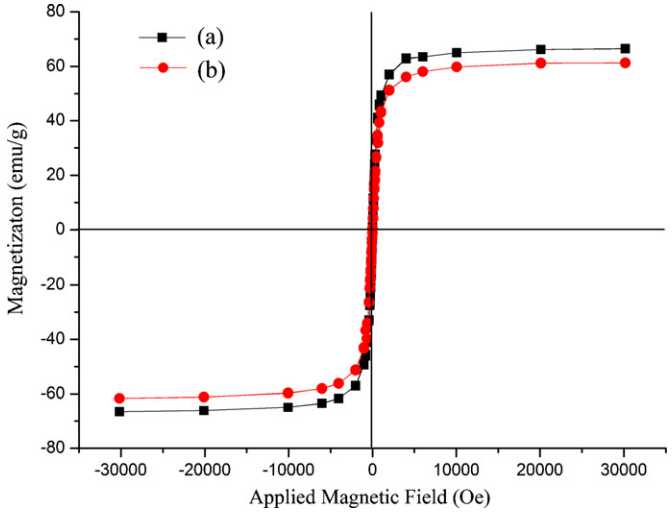

Fig. 5. Magnetization curve for the uncoated SPIO-NPs (a) and OCMCs-SPIO-NPs (b) at 300 K.

properties are critical in the applications of the pharmaceutical biomedical fields. When the magnetite nanoparticles undergo strong magnetization, the fixing magnetic materials at an objective site is allowed for, and when the applied magnet field is removed, redispersion of these nanoparticles will take place rapidly.

3.3. Functional studies of SP5.2/tTF-OCMCs-SPIO-NPs

3.3.1. The peptide-directed targeting study

In order to obtain the SP5.2/tTF-OCMCs-SPIO-NPs able to bind target cells, the peptide moiety SP5.2 must preserve its biological activity. Fig. 6 showed the binding and internalization of SP5.2/tTF-OCMCs-SPIO-NPs by laser scanning confocal microscope. In Fig. 6a, the SP5.2/tTF and SP5.2/tTF-OCMCs-SPIO-NPs treated groups both have the RBITC fluorescence signal and the signal intensities of SP5.2/tTF-OCMCs-SPIO-NPs group is stronger than the SP5.2/tTF group. On the contrary, there is no red fluorescence signal detected in the OCMCs-SPIO-NPs group. These results indicated that the fusion proteins SP5.2/tTF could bond with their receptors (VEGFR-1) on the cell's surface. The stronger RBITC fluorescence signal intensities in SP5.2/tTF-OCMCs-SPIO-NPs-treated group should be explained that SP5.2/tTF had already gathered on the OCMCs-SPIO-NPs surface and retained its bioactivity.

By Fig. 6b, the HUVECs incubated with SP5.2/tTF-OCMCs-SPIO-NPs for varying durations (1, 6 and 12 h). The RBITC fluorescence signal was detected only on the cell surface after 1 h incubation. However, 6 h later, little RBITC fluorescence signal was detected in the cytoplasm. Further on, stronger RBITC fluorescence signal was observed at 12 h after. That indicated the SP5.2/tTF-OCMCs-SPIO-NPs could be taken up into HUVECs dependent on incubation time. After binding to the cell surface, nanoparticle-base carriers should be internalized into intracellular space by the natural uptake process of endocytosis (Plank et al., 2011). But this should not influence the application of SP5.2/tTF-OCMCs-SPIO-NPs, because the coagulation cascade induced by tTF fusion proteins happens usually in minutes after administration.

3.3.2. The magnetic field-guided targeted study

Fig. 7 shows the cell culture experiment to evaluate the magnetic responsiveness of SP5.2/tTF-OCMCs-SPIO-NPs. Fig. 7a and b respectively shows the cells at circle 1 and circle 2 areas within the Petri dish by Prussian blue staining, and that referred circle 1 area is in the stronger magnetic field while the circle 2 area is much weaker. As visualized under microscopy, the circle 1 area (Fig. 7a) has stronger Prussian blue intensities than circle 2 area (Fig. 7b), which indicate that cells located inside circle 1 had taken up more SP5.2/tTF-OCMCs-SPIO-NPs than the cells located inside circle 1 after 6 h incubation. This result indicates that the SP5.2/tTF-OCMCs-SPIO-NPs should be guided to accumulate at a specific location by a permanent magnet.

3.3.3. The blood coagulation activity assay

To evaluation the retention of tTF-clotting activity of SP5.2/tTF-OCMCs-SPIO-NPs, Factor X activation assay and H&E histology analysis were performed, respectively *in vitro* and *in vivo*. As shown in Fig. 8a, SP5.2/tTF-OCMCs-SPIO-NPs and SP5.2/tTF have a similar activity of activating Factor X at the corresponding concentration. The ability of Factor X activation increased with the increase of drug concentration. When the concentration exceeded 1 μmol/l, the activities of SP5.2/tTF-OCMCs-SPIO-NPs began to be higher than the SP5.2/tTF. These demonstrated that the tTF moiety of SP5.2/tTF-OCMCs-SPIO-NPs not only remains the Factor X activation, but also might promote the blood coagulation.

H&E stained image (Fig. 8b) demonstrates that the tumor tissues of mice treated with SP5.2/tTF-OCMCs-SPIO-NPs or SP5.2/tTF were showed the thrombotic vessels and necrotic tumor tissue. By

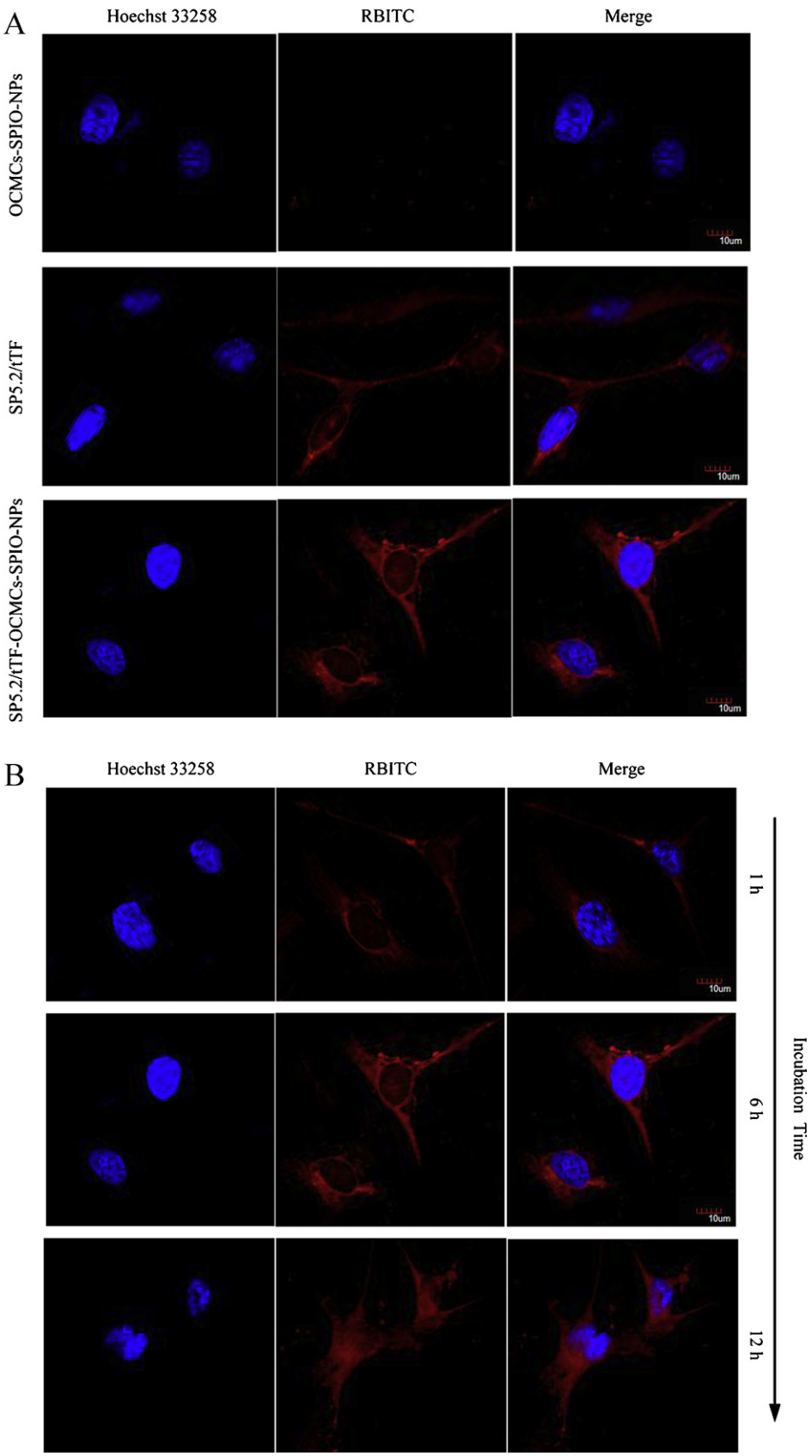

Fig. 6. Binding and internalization of SP5.2/tTF-OCMCs-SPIO-NPs by laser scanning confocal microscope analysis. (a) The HUVECs were cultured with OCMCs-SPIO-NPs (negative controls), SP5.2/tTF (positive controls) and SP5.2/tTF-OCMCs-SPIO-NPs for 6 h, respectively. As shown, SP5.2/tTF-OCMCs-SPIO-NPs still possess potent binding affinity to VEGFR-1-overexpressing HUVECs as the fusion protein SP5.2/tTF. (b) The HUVECs were treatment with SP5.2/tTF-OCMCs-SPIO-NPs for varying durations (1, 6 and 12 h). At 1 h point, it could be observed the SP5.2/tTF-OCMCs-SPIO-NPs bind to the cells surface.

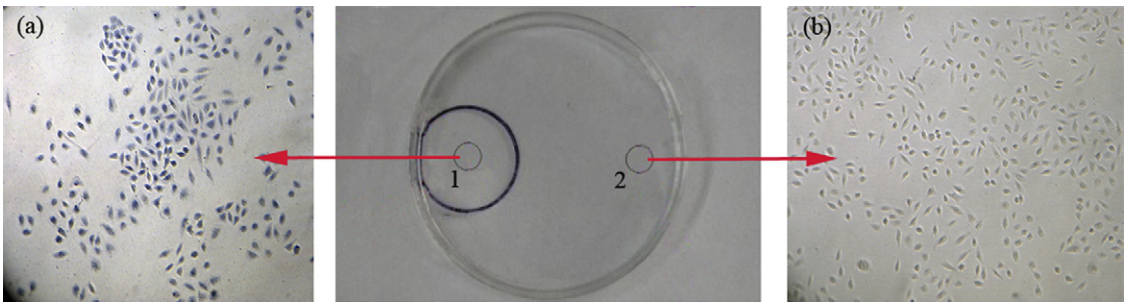

Fig. 7. Prussian blue staining analysis for the magnetic-induced targeting effect of SP5.2/tTF-OCMCs-SPIO-NPs in a different magnetic field. A 0.6 T permanent magnet was vertically placed at 1 cm distance from the Petri dish bottom marked as the large black circle, which supplied a higher magnetic field strength located in circle 1 than in circle 2. The cells image (a) display a stronger Prussian blue intensities than the image (b), which revealed a more accumulation of SP5.2/tTF-OCMCs-SPIO-NPs at a higher magnetic field strength area.

contrast, few induction of thrombosis was observed in the PBS-treated control group. Compared with SP5.2/tTF-treated group, a mass of the blood vessels in the tumor of SP5.2/tTF-OCMCs-SPIO-NPs-treated group was thrombosed and completely occluded, which also generated necrosis proximal to the site of occlusion. These results validly confirmed SP5.2/tTF-OCMCs-SPIO-NPs hold tTF-clotting activity *in vivo*. The similar approach by Simberg et al. (2007) showed that coupling magnetic nanoparticles with targeting peptide (CREKA) could be dragged to desired sites using external influence, and simultaneously induce the vessel occlusion.

The magnetite (Fe_3O_4) core endows the reagent with magnetic property, which able to be retained at the target site by a magnet field. Cylinder permanent magnets, electromagnets and Helmholtz loop all could be used for generating available magnetic field. Generally, the permanent magnets are placed directly against the tumor surface for building up sufficient field strength, and the distance between the magnet and the tumor is assured to be less than 0.5 cm (Lubbe et al., 2001). But the effect of magnetic drug targeting not only depends on the strength of the magnetic field but also the gradient of the magnetic field (Rudge et al., 2000). To increase the gradient of the magnetic field, the ferromagnetic wires are implanted at a diseased region generally, but the surgical injury subsequently (Lubbe et al., 2001; Ritter, 2004). In a word, these magnetic targeting devices each have advantages and disadvantages for clinical application and the ideal device remains to be further studied.

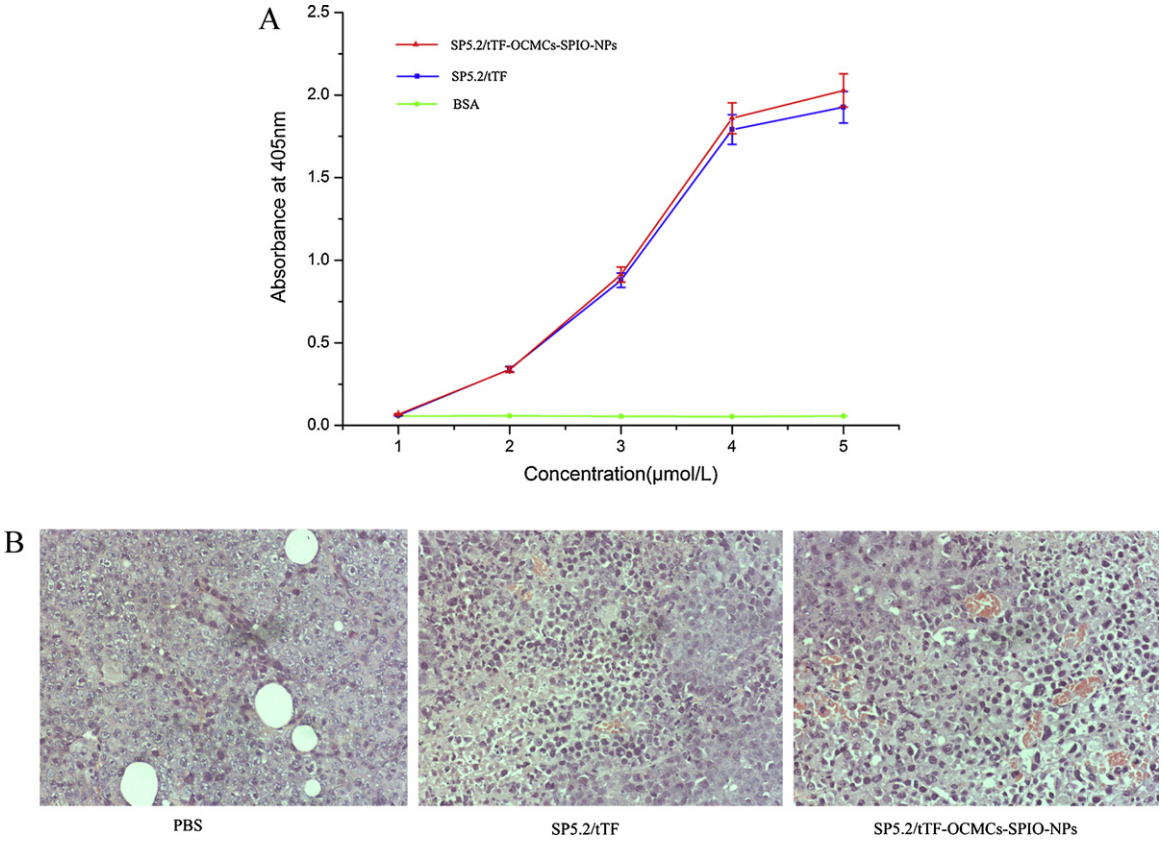

Fig. 8. The detection of tTF-coagulation activity of SP5.2/tTF-OCMCs-SPIO-NPs by Factor X coagulation assay and histological analyses. (a) Factor X coagulation assay, SP5.2/tTF-OCMCs-SPIO-NPs, SP5.2/tTF (positive control) and BSA (negative control). The SP5.2/tTF-OCMCs-SPIO-NPs obviously retained the tTF-clotting activity, even a slight enhancement compare with the SP5.2/tTF. (b) Histological analyses, histological comparison of thrombosed vessels mediated by tTF-based complexes in SMCC7721 tumors 48 h after treatment with PBS (negative control), SP5.2/tTF (positive control) and SP5.2/tTF-OCMCs-SPIO-NPs. A more complete tumor blood vessels thrombosis and necrotic tumor tissue were observed in the treatment with SP5.2/tTF-OCMCs-SPIO-NPs-treated group than SP5.2/tTF-treated group.

4. Conclusions

In conclusion, the SP5.2/tTF-OCMCs-SPIO-NPs with the size about 10–20 nm have successfully prepared. The results demonstrated that the OCMCs-SPIO-NPs were of the superparamagnetic properties and functional carboxyl groups. Moreover, SP5.2/tTF-OCMCs-SPIO-NPs achieved an efficient double-targeting to HUVECs or tumor cells and activation blood coagulation *in vitro* and *in vivo*. The modification of SPIO-NPs with OCMCs and SP5.2/tTF is a promising method to improve the stability and specific VEGFR-1 tumor-target of SPIO-NPs, thus boosting the application of SP5.2/tTF-OCMCs-SPIO-NPs in embolization therapy of tumor blood vessels.

Acknowledgments

This work was supported by the National Natural Science Foundation of China (Grant Nos. 30973485, and 81172970).

References

Ai, J.-H., Zheng, S.-G., Zeng, Y.-Y., Xiong, Y., Zhang, L.-d., Dong, J.-H., 2008. The expression and significance of vascular endothelial growth factor and its receptors in hepatocellular carcinoma cell lines with various metastatic potentialities. Zhonghua gan zang bing za zhi = Zhonghua ganzangbing zazhi 16, 105–108.

Berry, C.C., Charles, S., Wells, S., Dalby, M.J., Curtis, A.S.G., 2004. The influence of transferrin stabilised magnetic nanoparticles on human dermal fibroblasts in culture. Int. J. Pharm. 269, 211–225.

Carmeliet, P., 2000. Mechanisms of angiogenesis and arteriogenesis. Nat. Med. 6, 389–395.

Corot, C., Robert, P., Idee, J.-M., Port, M., 2006. Recent advances in iron oxide nanocrystal technology for medical imaging. Adv. Drug Deliv. Rev. 58, 1471–1504.

Folkman, J., 1995. Angiogenesis in cancer, vascular, rheumatoid and other disease. Nat. Med. 1, 27–31.

Folkman, J., Watson, K., Ingber, D., Hanahan, D., 1989. Induction of angiogenesis during the transition from hyperplasia to neoplasia. Nature 339, 58–61.

Furie, B., Furie, B.C., 1988. The molecular basis of blood coagulation. Cell 53, 505–518.

Gille, H., Kowalski, J., Li, B., LeCouter, J., Moffat, B., Zioncheck, T.F., Pelletier, N., Ferrara, N., 2001. Analysis of biological effects and signaling properties of Flt-1 (VEGFR-1) and KDR (VEGFR-2) – a reassessment using novel receptor-specific vascular endothelial growth factor mutants. J. Biol. Chem. 276, 3222–3230.

Goncalves, V., Gautier, B., Garbay, C., Vidal, M., Inguimbert, N., 2007a. Development of a chemiluminescent screening assay for detection of vascular endothelial growth factor receptor 1 ligands. Anal. Biochem. 366, 108–110.

Goncalves, V., Gautier, B., Regazzetti, A., Coric, P., Bouaziz, S., Garbay, C., Vidal, M., Inguimbert, N., 2007b. On-resin cyclization of peptide ligands of the vascular endothelial growth factor receptor 1 by copper(I)-catalyzed 1,3-dipolar azide–alkyne cycloaddition. Bioorg. Med. Chem. Lett. 17, 5590–5594.

Hanahan, D., Folkman, J., 1996. Patterns and emerging mechanisms of the angiogenic switch during tumorigenesis. Cell 86, 353–364.

Hong, R.Y., Feng, B., Chen, L.L., Liu, G.H., Li, H.Z., Zheng, Y., Wei, D.G., 2008a. Synthesis, characterization and MRI application of dextran-coated Fe_3O_4 magnetic nanoparticles. Biochem. Eng. J. 42, 290–300.

Hong, R.Y., Li, J.H., Li, H.Z., Ding, J., Zheng, Y., Wei, D.G., 2008b. Synthesis of Fe_3O_4 nanoparticles without inert gas protection used as precursors of magnetic fluids. J. Magn. Magn. Mater. 320, 1605–1614.

Hu, P., Yan, J., Sharifi, J., Bai, T., Khawli, L.A., Epstein, A.L., 2003a. Comparison of three different targeted tissue factor fusion proteins for inducing tumor vessel thrombosis. Cancer Res. 63, 5046–5053.

Hu, P.S., Yan, J.H., Sharifi, J., Bai, T., Khawli, L.A., Epstein, A.L., 2003b. Comparison of three different targeted tissue factor fusion proteins for inducing tumor vessel thrombosis. Cancer Res. 63, 5046–5053.

Huang, X.M., Molema, G., King, S., Watkins, L., Edgington, T.S., Thorpe, P.E., 1997. Tumor infarction in mice by antibody-directed targeting of tissue factor to tumor vasculature. Science 275, 547–550.

Ito, A., Shinkai, M., Honda, H., Kobayashi, T., 2005. Medical application of functionalized magnetic nanoparticles. J. Biosci. Bioeng. 100, 1–11.

Jain, T.K., Morales, M.A., Sahoo, S.K., Leslie-Pelecky, D.L., Labhasetwar, V., 2005. Iron oxide nanoparticles for sustained delivery of anticancer agents. Mol. Pharm. 2, 194–205.

Krukemeyer, M.G., Krenn, V., Jakobs, M., Wagner, W., 2011. Mitoxantrone–iron oxide biodistribution in blood, tumor, spleen, and liver-magnetic nanoparticles in cancer treatment. J. Surg. Res., doi:10.1016/j.jss.2011.01.060.

Lei, Z., Pang, X., Li, N., Lin, L., Li, Y., 2009. A novel two-step modifying process for preparation of chitosan-coated Fe(3)O(4)/SiO(2) microspheres. J. Mater. Process. Technol. 209, 3218–3225.

Lind, K., Kresse, M., Debus, N.P., Muller, R.H., 2002. A novel formulation for superparamagnetic iron oxide (SPIO) particles enhancing MR lymphography: comparison of physicochemical properties and the in vivo behaviour. J. Drug Target. 10, 221–230.

Liu, H.Z., Ma, Z.Y., Guan, Y.P., 2005. Synthesis and characterization of micron-sized monodisperse superparamagnetic polymer particles with amino groups. J. Polym. Sci. Part A: Polym. Chem. 43, 3433–3439.

Lubbe, A.S., Alexiou, C., Bergemann, C., 2001. Clinical applications of magnetic drug targeting. J. Surg. Res. 95, 200–206.

Molday, R.S., MacKenzie, D., 1982. Immunospecific ferromagnetic iron–dextran reagents for the labeling and magnetic separation of cells. J. Immun. Methods 52, 353–367.

Morrissey, J.H., Macik, B.G., Neuenschwander, P.F., Comp, P.C., 1993. Quantitation of activated factor VII levels in plasma using a tissue factor mutant selectively deficient in promoting factor VII activation. Blood 81, 734–744.

Plank, C., Zelphati, O., Mykhaylyk, O., 2011. Magnetically enhanced nucleic acid delivery. Ten years of magnetofection – progress and prospects. Adv. Drug Deliv. Rev. 63, 1300–1331.

Ritter, J., 2004. Application of high gradient magnetic separation principles to magnetic drug targeting. J. Magn. Magn. Mater. 280, 184–201.

Rudge, S.R., Kurtz, T.L., Vessely, C.R., Catterall, L.G., Williamson, D.L., 2000. Preparation, characterization, and performance of magnetic iron–carbon composite microparticles for chemotherapy. Biomaterials 21, 1411–1420.

Ruf, W., Rehemtulla, A., Morrissey, J.H., Edgington, T.S., 1991. Phospholipid-independent and -dependent interactions required for tissue factor receptor and cofactor function. J. Biol. Chem. 266, 2158–2166.

Schweiger, C., Pietzonka, C., Heverhagen, J., Kissel, T., 2011. Novel magnetic iron oxide nanoparticles coated with poly(ethylene imine)-g-poly(ethylene glycol) for potential biomedical application: synthesis, stability, cytotoxicity and MR imaging. Int. J. Pharm. 408, 130–137.

Schwoeppe, C., Kessler, T., Persigehl, T., Liersch, R., Hintelmann, H., Dreischalueck, J., Ring, J., Bremer, C., Heindel, W., Mesters, R.M., Berdel, W.E., 2010. Tissue-factor fusion proteins induce occlusion of tumor vessels. Thromb. Res. 125, S143–S150.

Shubayev, V.I., Pisanic, T.R., Jin I.I., S., 2009. Magnetic nanoparticles for theragnostics. Adv. Drug Deliv. Rev. 61, 467–477.

Simberg, D., Duza, T., Park, J.H., Essler, M., Pilch, J., Zhang, L., Derfus, A.M., Yang, M., Hoffman, R.M., Bhatia, S., Sailor, M.J., Ruoslahti, E., 2007. Biomimetic amplification of nanoparticle homing to tumors. Proc. Natl. Acad. Sci. U.S.A. 104, 932–936.

Stone, M.J., Ruf, W., Miles, D.J., Edgington, T.S., Wright, P.E., 1995. Recombinant soluble human tissue factor secreted by *Saccharomyces cerevisiae* and refolded from *Escherichia coli* inclusion bodies: glycosylation of mutants, activity and physical characterization. Biochem. J. 310, 605–614.

Yang, X., Chen, Y., Yuan, R., Chen, G., Blanco, E., Gao, J., Shuai, X., 2008. Folate-encoded and Fe_3O_4-loaded polymeric micelles for dual targeting of cancer cells. Polymer 49, 3477–3485.

Zhou, L.-M., Wang, Y.-P., Liu, Z.-R., Huang, Q.-W., 2006. Carboxymethyl chitosan–Fe_3O_4 nanoparticles: preparation and adsorption behaviors towards Zn^{2+} ions. Acta Phys. Chim. Sin. 22, 1342–1346.

Zhu, A., Yuan, L., Liao, T., 2008. Suspension of Fe_3O_4 nanoparticles stabilized by chitosan and o-carboxymethylchitosan. Int. J. Pharm. 350, 361–368.